Dynamics of protein condensates in weak-binding regime

Ya-Xin Xiang,[*] Yue Shan,[*] Qun-Li Lei, Chun-Lai Ren,[†] and Yu-Qiang Ma[‡]
National Laboratory of Solid State Microstructures and Department of Physics, and Collaborative Innovation Center of Advanced Microstructures, Nanjing University, Nanjing 210093, China

(Received 14 April 2022; accepted 19 September 2022; published 10 October 2022)

Weak complementary interactions between proteins and nucleic acids are the main driving forces of intracellular liquid-liquid phase separation. The sticker-spacer model has emerged as a unifying principle for understanding the phase behavior of these multivalent molecules. It remains elusive how specific interactions mediated by stickers contribute to the rheological properties of the liquid condensates. Previous studies have revealed that for strong binding strength ε_b, the bulk diffusivity D depends on the effective bond lifetime τ, viz., $D \propto \tau^{-1}$. Consequently, equal concentrations of the complementary stickers induce a slow down in the dynamics of the condensates $D \propto e^{-1.5\varepsilon_b}$. However, for weak-binding strength, it is expected that the resulting condensates are dynamic, loose network liquids rather than kinetically arrested, compact clusters. We develop a mean-field theory using the thermodynamics of the associative polymers and perform molecular-dynamics simulations based on the sticker-spacer model to study the controlling factors in the structure and dynamics of such condensates in the weak-binding regime. Through scaling analysis, we delineate how the free sticker fraction W_f and the bulk diffusivity D decrease with increasing binding energy and find that the internal dynamics of such network liquids are controlled by the free sticker fraction $D \propto W_f \propto e^{-0.5\varepsilon_b}$ rather than the effective bond lifetime. Referred to as the free-sticker-dominated diffusivity, the microscopic slowdown due to a gradual loss of the free stickers affects the viscosity of the condensates as well, with the scaling of the zero-shear viscosity $\eta \propto e^{0.5\varepsilon_b}$. Therefore, the way of controlling the structure, diffusivity, and viscosity of the condensates through the binding energy can be tested experimentally.

DOI: 10.1103/PhysRevE.106.044403

I. INTRODUCTION

Liquid-liquid phase separation (LLPS) driven by multivalent proteins and nucleic acids has emerged as a general solution utilized by cells to realize intracellular spatiotemporal organization [1–5]. Depending on factors such as pH, ATP, chaperones, and salt concentrations, these protein-rich condensates exhibit tunable liquidity [2,6–15] and can mature over time [16–19]. Loss of internal dynamics and subsequent solidification are often implicated in diseases [8,20–23]. Despite the crucial significance of condensates dynamics, its molecular origins remain unclear. A recent experimental study suggests that protein condensates are viscoelastic Maxwell fluids with age-dependent material properties [16]. Questions have arisen regarding the molecular underpinnings of the macroscopic rheologic properties.

Recent studies have established that proteins harboring intrinsically disordered regions are the main drivers of intracellular LLPS [11,24–26], whose phase behaviors have been analyzed based on the sticker-spacer model for associative polymers [26–31]. This coarse-grained model is based on the dichotomy between domains involved in specific interactions (stickers) and those involved in nonspecific interactions (spacers) [28]. The composition of the condensates is dictated by the sequence encoded interactions as well. For example, many protein-RNA condensates are reported to form via the process of complex coacervation [7,18].

Associative polymers can form network liquids (physical gels) through specific noncovalent interactions among the stickers. Crucially, such network fluids bear some resemblance to the phenomenological Maxwell fluids, in that both possess viscoelastic properties and characteristic time scales (relaxation times). The sticker-spacer paradigm can thus be developed to uncover the invisible microscopic processes dictating the macroscopic relaxation times. Although the solubility of the spacers affects both the compactness of such network liquids and lower threshold concentrations for phase separation as well [29,32], one can expect that for dilute protein condensates [10,33], the dynamics of such bond network is controlled by stickers. Ronceray *et al.* recently showed that in systems driven by strong, complementary interactions, the bulk diffusivity decreases significantly at balanced stoichiometry, due to a substantial increase in the bond lifetime as free stickers become sparse [34]. We refer to the mechanism as the bond-breakage-limited diffusivity.

While much emphasis has been put on the strong-binding regime, the weak-binding regime receives less attention. Does the bond-breakage-limited diffusivity hold in the weak-binding regime? What is the leading factor that controls the structure and dynamics of the liquid condensates in this

[*]These authors contributed equally to this work.
[†]Corresponding author: chunlair@nju.edu.cn
[‡]Corresponding author: myqiang@nju.edu.cn

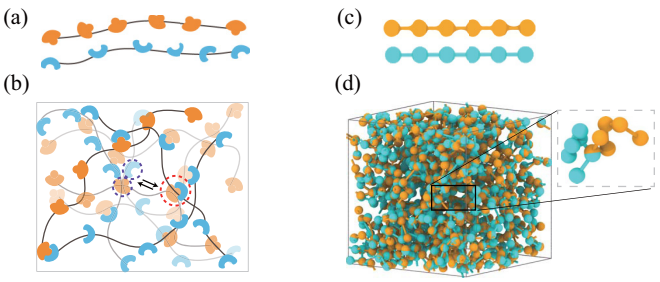

FIG. 1. (a) Schematic of multivalent proteins with associative domains (A colored in blue and B in orange). (b) Depiction of liquid network within dense phase stabilized by transient intermolecular bonds, where the weak-binding energy allows coexistence of bound (dashed black circle) with free (dashed purple circles) stickers. (c) MD model for multivalent proteins. (d) A simulation snapshot of dense phase as an open network, with many free stickers (as shown in its enlargement).

regime? In this work, we try to answer these questions. We develop a mean-field theory to relate the free sticker fraction to the diffusivity and disscuss the the rationale behind the free-sticker-dominated diffusivity. We then study the dynamics of associative polymers with complementary stickers via molecular-dynamics simulations, from which we estimate bond relaxation times, self-diffusivity, viscosity, and free sticker fraction. We find that the ability of stoichiometry to control bond fraction is compromised by the weak binding strength, as we observe the coexistence of free and bound stickers at equal valences and balanced stoichiometry. The bulk diffusivity is proportional to the free sticker fraction, rather than the reciprocal of the bond lifetime, in agreement with the expected scaling behavior of the free-sticker-dominated mechanism of dynamics slowdown.

II. MEAN-FIELD THEORY

We consider a system consisting of two types of chains, each composed of either m_A sticker A or m_B sticker B, as schematized in Fig. 1(a), where m_A, m_B are referred to as valences. Each sticker can form one and only one bond with its partner of binding energy $-\varepsilon_b$ (in the unit of k_BT). In the weak-binding regime, free stickers coexist with bound stickers, as highlighted in the purple and black circle(s) in Fig. 1(b), respectively. In addition to binding energy, there are three control parameters, namely the difference in valence between two kinds of chains $\Delta m = m_A - m_B$, sticker total concentration $n = n_A + n_B$, and stoichiometry $\delta = n_A - n_B$, where n_A and n_B is the number density of A and B.

Let V be the volume of the box. The partition function of forming N_b bonds out of Vn_A A stickers and Vn_B B stickers is [32]

$$Z(N_b) = PW_{\text{Bonds}}, \tag{1}$$

where W_{Bonds} is the number of different ways to select N_b pairs of stickers, which reads

$$W_{\text{Bonds}} = \binom{Vn_A}{N_b}\binom{Vn_B}{N_b}N_b!. \tag{2}$$

P is the probability that N_b stickers are close to their partners and form N_b bonds, assuming that formation of bonds is independent of one another:

$$P = \left(\frac{v_0}{V}\right)^{N_b} e^{N_b\varepsilon_b}, \tag{3}$$

where the volume of sticker $v_0 = 4\pi r_0^3/3$, and V is the volume of the box.

The free energy density is

$$\begin{aligned}\beta f &= -\frac{1}{V}\ln(Z)\\ &= \phi_B[(1-p_B)\ln(1-p_B) + p_B\ln(p_B)]\\ &\quad + \phi_A\left[(1-p_A)ln(1-p_A) - p_A\ln\left(\frac{\phi_A}{e}\right) - p_A\varepsilon_b\right],\end{aligned} \tag{4}$$

where $p_i = N_b/N_i$, $\phi_i = n_i v_0$, $i = A, B$ is the bond fraction and the volume fraction of sticker i, respectively.

The number of bound A equals the number of bound B :

$$p_A\phi_A = p_B\phi_B. \tag{5}$$

Minimization of the free energy density with respect to the bond fraction p_A, p_B yields the detailed balance condition

$$e^{-\varepsilon_b}p_B\phi_B = (1-p_B)(1-p_A)\phi_A\phi_B. \tag{6}$$

We express bond fraction as a function of the difference in concentration between the two components $\delta v_0 = \phi_A - \phi_B$ and their total concentration $\phi = \phi_A + \phi_B$ as

$$p_A = \frac{\phi + e^{-\varepsilon_b}}{\phi + \delta v_0} - \sqrt{\left(\frac{\phi + e^{-\varepsilon_b}}{\phi + \delta v_0}\right)^2 - \frac{\phi - \delta v_0}{\phi + \delta v_0}}, \tag{7}$$

$$p_B = \frac{\phi + e^{-\varepsilon_b}}{\phi - \delta v_0} - \sqrt{\left(\frac{\phi + e^{-\varepsilon_b}}{\phi - \delta v_0}\right)^2 - \frac{\phi + \delta v_0}{\phi - \delta v_0}}. \tag{8}$$

The free sticker concentration is written:

$$\begin{aligned}W_f &= (1-p_A)\frac{\phi_A}{\phi} + (1-p_B)\frac{\phi_B}{\phi}\\ &= \frac{2\sqrt{n_{AB}}}{n}v_0^{-0.5}e^{-0.5\varepsilon_b}\left(1 + \frac{v_0\delta^2}{4n_{AB}e^{-\varepsilon_b}}\right)^{0.5},\end{aligned} \tag{9}$$

where $n_{AB} = N_b/V$ is the density of bonds. We can infer from Eq. (9) that extremely imbalanced stoichiometry is sufficient to fluidify condensates, in which case the effect of binding strength is screened out and the fraction of free stickers is that of the sticker in excess. On the contrary, at nearly balanced stoichiometry, the free sticker fraction shows a strong dependence on the binding energy, viz.,

$$W_f \approx \begin{cases} \frac{|\delta|}{n}, & v_0\delta^2 \gg n_{AB}e^{-\varepsilon_b} \\ \frac{2\sqrt{n_{AB}}}{n}v_0^{-0.5}e^{-0.5\varepsilon_b}, & v_0\delta^2 \ll n_{AB}e^{-\varepsilon_b}. \end{cases} \tag{10}$$

The probability $P(n_f)$ that a chain $m_A = m$ has n_f free stickers is given by the binomial distribution, which is the most probable distribution given the average bond fraction:

$$P(n_f) = \binom{m}{n_f}(1-p_A)^{n_f}p_A^{m-n_f}. \tag{11}$$

Substation of p_A in Eq. (11) for its equilibrium value given in Eq. (7) yields the theoretical predictions.

To relate the equilibrium structure to the dynamics of the condensates, we assume that the free and bound stickers contribute independently to the diffusivity and decompose the diffusion coefficient D into two parts accordingly. There are only intermolecular bonds in such systems and thus all bonds contribute equally to the macroscopic dynamics. Namely, we propose the following expression for the diffusivity:

$$D = D_0\Big[W_f + (1 - W_f)\frac{\tau_0}{\tau}\Big], \tag{12}$$

where D_0 is the diffusivity of a free sticker given by $D_0 = r_0^2/\tau_0$ and τ_0 is a microscopic time and the free sticker fraction W_f given in Eq. (9) and (10). The effective bond lifetime τ can be expressed as [34]

$$\tau = \tau_0 e^{\varepsilon_b}\left[1 + \frac{1}{v_{\text{cage}} W_f}\right]. \tag{13}$$

The denominator of the second addend $W_f v_{\text{cage}} \gg 1$ in the weak-binding regime, due to the fast internal dynamics and an abundance of free stickers. Dropping the second addend in Eq. (13) yields

$$\tau \approx \tau_0 e^{\varepsilon_b}. \tag{14}$$

In the strong-binding regime, the former two partners may rebind to each other many times, until either of them finds a new partner, thus the diffusion coefficient approaches the inverse effective bond lifetime $D \approx \tau^{-1}$.

In the weak-binding regime, however, the probability that either of the two former partners binds to another nearby partner immediately after a bond-breaking event is small, $(1 - W_f)\tau^{-1} \ll W_f \tau_0^{-1}$; the scaling of the diffusion coefficient echoes that of the free sticker fraction. We refer to the microscopic mechanism as the free-sticker-dominated diffusivity, which predicts that

$$D \propto W_f. \tag{15}$$

Under the condition of nearly balanced stoichiometry, the prefactor in Eq. (10) varies relatively slowly, hence the free sticker fraction decreases with the binding energy as

$$W_f \propto e^{-0.5\varepsilon_b}. \tag{16}$$

Combining Eq. (16) with Eq. (15), we obtain

$$D \propto e^{-0.5\varepsilon_b}. \tag{17}$$

The scaling behavior given by Eqs. (15)–(17) is our central prediction.

III. MOLECULAR-DYNAMICS SIMULATION

To validate our predictions within a more realistic multivalent protein framework, we adopt the model used in [34] and perform molecular-dynamics (MD) simulations of a two-component mixture of bead-spring polymers, where each bead represents a sticker, as sketched in Fig. 1(c).

The beads are connected by finite extensible nonlinear elastic (FENE) bonds described by the following potential:

$$E_b(r) = -\frac{KR_0^2}{2}\ln\left[1 - \left(\frac{r}{R_0}\right)^2\right]. \tag{18}$$

We set the stiffness coefficient $K = 3$, and the maximum extent of the bond $R_0 = 3$.

To enable association between a pair of stickers, an attractive potential is applied to them, which reads

$$E_a(r) = \begin{cases} E_0\Big[1 + \cos\Big(\dfrac{\pi r}{r_c}\Big)\Big], & r < r_c \\ 0, & r \geqslant r_c \end{cases}, \tag{19}$$

where the interaction strength E_0 is negative, indicating a well between the complementary stickers of width r_c. We set the cutoff to $r_c = 0.3$.

The binding energy ε_b is related to the interaction strength E_0, via

$$\varepsilon_b = \ln\left(\frac{\int_0^{r_c} 4\pi r^2 e^{-E_a(r)} dr}{4\pi r_c^3/3}\right), \tag{20}$$

with E_0 being negative, the Boltzmann factor of forming a bond if the distance between a sticker and its partner is smaller than r_c is greater than one, $e^{-E_a(r)} > 1$. Thus, the integral ε_b is positive, and the binding energy $-\varepsilon_b$ is negative.

To ensure that a bond forms only between a pair of complementary stickers, we simulate the repulsive interactions between stickers of the same type through the truncated Lennard-Jones potential which reads

$$E_r(r) = \begin{cases} 4\varepsilon\big[\big(\frac{\sigma}{r}\big)^{12} - \big(\frac{\sigma}{r}\big)^{6}\big], & r < r_c \\ 0, & r \geqslant r_c \end{cases}. \tag{21}$$

We set $r_c = 2^{1/6}\sigma$, and $\varepsilon = 1$, $\sigma = 0.6$. The equilibrium linker length r_0 is determined by the force balance condition $\partial_r E_b = -\partial_r E_r$, which yields $r_0 \approx 1.12\sigma$.

We simulate systems with either unequal valences or imbalanced stoichiometry at fixed concentrations, and systems with different concentrations at equal valences and stoichiometry. In each case, we systematically vary the binding energy. We use normalized energy $k_B T = 1$ and set the bead mass $m = 1$. Simulations are performed on an NVT ensemble with Langevin thermostat at $T = 1.0$ in a cubic box of volume $V = 10^3$ with the periodic boundary conditions in all directions. We set the damping parameter to 0.5 and the time step to 0.005. We first anneal the systems via varying E_0 from zero to its final value in 10^8 time steps, and then simulate again for 10^6 time steps for relaxation. We repeat the simulation 10 times for each binding energy. For each replica, we average the results over 10^4 data points. Statistical error bars are smaller than the symbol size. Simulations were performed using the LAMMPS software package [35].

IV. RESULTS

We first deploy MD simulations to query the impacts of binding energy on condensates structure. In the weak-binding regime, equal valences ($\Delta m = 0$) and balanced stoichiometry ($\delta = 0$) cannot ensure exhaustion of free stickers [Fig. 1(d)]. According to the Flory-Stockmayer theory [36,37], a system-spanning network emerges from a solution of dispersed monomers and oligomers as the average bond fraction achieves a threshold value, known as the gel point. We measure the average bond fraction of the two components and determine their relative distance to the gel point, which is

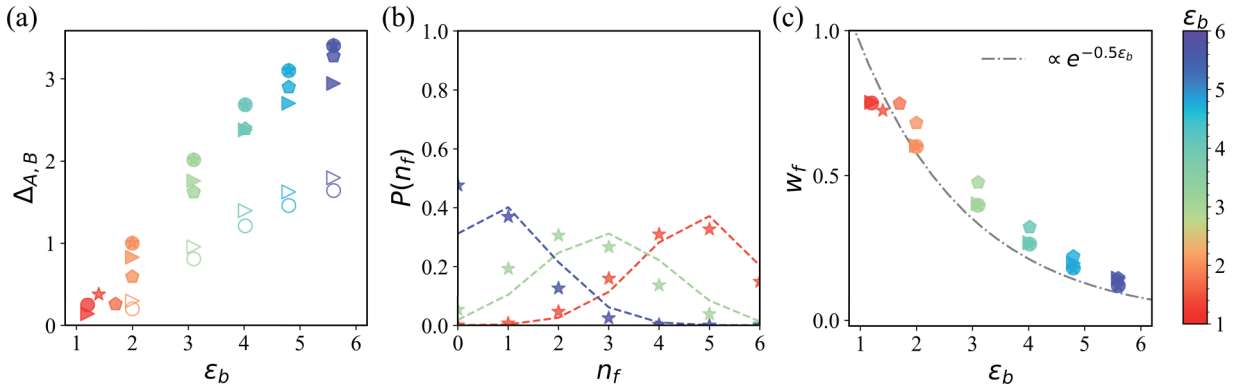

FIG. 2. (a) Relative distance to the gel point for A (filled symbols) and B (open symbols) as a function of binding energy. (b) Probability distribution of a chain ($m_A = 6$) carrying n_f free stickers. Symbols are MD simulations and dashed lines are binomial distributions predicted by theory [Eq. (11)]. (c) The free sticker fraction as a function of the binding energy. Parameters for all plots read: For stars, $m_A = m_B = 6, n = 1.73, \delta = 0$; for triangles, $m_A = 6, m_B = 4, n = 1.73, \delta = 1.4$; for pentagons, $m_A = m_B = 6, n = 1.2, \delta = 0$; and for circles, $m_A = 6, m_B = 4, n = 1.73, \delta = 0$. Different colors correspond to different binding energy.

given by

$$\Delta_i = \frac{n_{AB}}{n_i p_{gi}} - 1, \tag{22}$$

where $p_{gi} = 1/(m_i - 1)$, $i = A, B$ is the gel point based on the Flory-Stockmayer theory [36,37] and n_{AB} is the density of bonds. We plot the results in Fig. 2(a), from which we find that the bond fraction of the two components is above the gel point $\Delta_{A,B} > 0$ in all systems, indicating that a condensate-spanning network occurs.

Due to the rapid internal dynamics, physical gels in the weak-binding regime are equilibrium structures as opposed to the metastable clusters in the strong-binding regime [38]. It then follows that for a given chain, the probability distribution of the number of bonds it forms confirms to a binomial distribution. We then determine the probability distribution $P(n_f)$ of a single chain ($m_A = 6$) with n_f free stickers from the MD simulations [symbols in Fig. 2(b), the length of errorbar is smaller than the symbol size], which is in good agreement with the theoretically predicted binomial distributions [dashed lines in Fig. 2(b), explicit expression given by Eq. (11)]. Thus, the mean-field treatment relates the structure features to the molecular interactions in the weak-binding regime.

For network liquids, there is an effective mesh size that dictates the size-scale dependent molecular permeability, visualized by the size dependent viscosity of probe particles [33], as is the case for other complex fluids [39,40]. Probes that are much smaller than the effective mesh size are blind to the presence of the polymer networks. The viscosity due to the surrounding networks increases with increasing probe radius and approaches a plateau value. The effective mesh size ξ can be characterized by the average distance between bonds, analogous to that between the points of entanglement in semidilute polymer solutions [39]. Assume that a typical section of a chain between interchain bonds is much larger than correlation blob strand, a scaling picture yields $\xi_i \approx R_g^i (m_i p_i)^{-1/2}$. Above the gel point, there is $(m_i p_i)^{-1/2} < (m_i p_{gi})^{-1/2} < 1, i = A, B$, implying that the effective mesh size is smaller than the size of the polymer coil R_g^i and decreases as the relative distance of the bond fraction to the gel point increases. Decreasing binding energy leads to a looser network, as indicated by the right shift of $P(n_f)$ and smaller relative distance to the gel point $\Delta_{A,B}$.

The degree of looseness is also reflected in the free sticker fraction $W_f = 1 - 2n_{AB}/n$. Under the condition of nearly balanced stoichiometry, we expect that the free sticker fraction decreases with the binding energy as $W_f \propto e^{-0.5\varepsilon_b}$ [dashed line in Fig. 2(c)]. Simulation results confirm the scaling [symbols in Fig. 2(c)].

We then characterize the dynamics of condensates. To aid comparison, we take the time τ_0 took for a sticker to diffuse a distance of the equilibrium linker length r_0 as the unit of time $\tau_0 = 1$. We quantify the bond relaxation process through estimation of the average bond lifetime τ via [34]

$$\tau = \int_0^\infty \frac{C(\Delta t)}{C(0)} d\Delta t, \tag{23}$$

where Δt is the lag time and $C(\Delta t)$ the autocorrelation functions given by

$$C(\Delta t) = \left\langle \sum_{i,j} A_{ij}(t) A_{ij}(t + \Delta t) \right\rangle_t. \tag{24}$$

The bond adjacency matrix $A_{ij}(t)$ vanishes except that at time t, the distance between sticker i and j is less than the attractive range r_c. The probability that a bond formed at $t = 0$ does not break at $t = \Delta t$ can be approximated by the normalized autocorrelation function

$$c(\Delta t) = \frac{C(\Delta t)}{C(0)}. \tag{25}$$

We can infer from Fig. 3(a) that, as binding strength increases, bonds are reversible since all curves decay to zero, while harder to break, as $c(\Delta t)$ becomes greater. Prior studies reported that equal valences and balanced stoichiometry lead to a sizable increase in bond lifetime $\tau \gg e^{\varepsilon_b}$ [34,38]. In contrast, we find that $\tau \propto e^{\varepsilon_b}$, indicating that the effect of both factors on bond lifetime is negligible [Fig. 3(b)].

To characterize the liquidity of the condensates, we first record the average mean squared displacement (MSD) of stickers as a function of the lag time. The results are shown

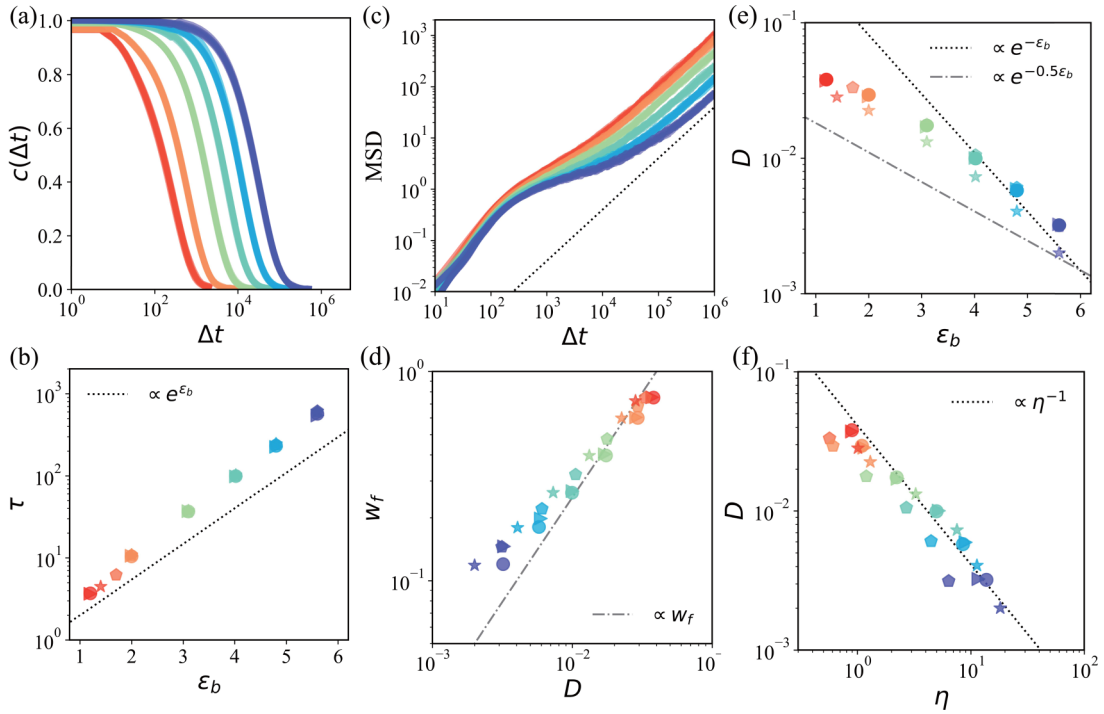

FIG. 3. (a) Normalized average autocorrelation plotted against lag time. (b) Bond lifetime as a function of binding energy. (c) Mean squared displacement (MSD) of all stickers as a function of lag time, where the dotted line indicates the normal diffusive scaling MSD(t) $\propto t$. (d) Correlation between diffusion coefficient and free sticker fraction, where dashed line indicates a linear relation. (e) Diffusion coefficient as a function of binding energy. (f) Viscosity obtained via the Green-Kubo relation and long-time diffusion coefficient of stickers confirm the Einstein relation, $D \propto \eta^{-1}$. Parameters for symbols read as follows: for stars, $m_A = m_B = 6, n = 1.73, \delta = 0$; for triangles, $m_A = 6, m_B = 4, n = 1.73, \delta = 1.4$; for pentagons, $m_A = m_B = 6, n = 1.2, \delta = 0$; and for circles, $m_A = 6, m_B = 4, n = 1.73, \delta = 0$. Colors code for the binding energy. Parameters for (a) and (c): $m_A = m_B = 6, n = 1.73, \delta = 0$.

in Fig. 3(c), where the short-time MSD represents vibration of stickers. The longtime MSD increases linearly with lag time, confirming the diffusive scaling [dotted line in Fig. 3(c)], suggesting that the condensates behave like liquids, unlike elastic solids, where the atoms can only vibrate about their equilibrium position. The width of the plateau in between indicates the relaxation time. As the binding energy increases, the plateau becomes wider, and the time scale on which the condensates exhibit liquidlike behavior becomes longer.

We extract the long-time diffusion coefficient D from MSD by linear fitting. We find that the long-time diffusion coefficient correlates with the free sticker fraction [Fig. 3(d)] and that as the binding energy increases, the diffusivity decreases as $D \propto e^{-0.5\varepsilon_b}$ [dash-dot line in Fig. 3(e)], which echo our theoretical predictions that the diffusivity is controlled by the fraction of the free stickers [Eqs. (15) and (17)]. Furthermore, our data deviate from the reciprocal relation $D \propto \tau^{-1} \propto e^{-\varepsilon_b}$ [dotted line in Fig. 3(e)], which is the signature of the bond-breakage-limited diffusivity [34]. Besides, slightly imbalanced stoichiometry [triangles in Fig. 3(e)] and lower concentration [pentagons in Fig. 3(e)] lead to a slight increase in diffusivity without altering the aforementioned scaling. The difference between equal and unequal valences [stars and circles in Fig. 3(e), respectively] in the diffusivity is negligible. Taken together, in the weak-binding regime, there is a novel route to slowing dictated by the free sticker fraction rather than the bond lifetime.

We then estimate the zero-shear viscosity from pressure fluctuations from equilibrium simulations. The Green-Kubo relation for the equilibrium shear viscosity reads [41]

$$\eta = \frac{V}{k_B T} \int_0^\infty \langle P_{ij}(t) P_{ij}(t + t') \rangle_t dt', \tag{26}$$

where i and $j = x, y, z$, and P_{ij} is one of the three components of the traceless symmetric part of of the pressure tensor, P_{xy}, P_{yz}, P_{xz}. The equation for P_{ij} is given by [41]

$$P_{ij} = \frac{1}{V} \sum_{\alpha=1}^{N} m_\alpha v_{\alpha i} v_{\alpha j} + \frac{1}{V} \sum_{\alpha=1}^{N} r_{\alpha i} F_{\alpha j}, \tag{27}$$

where N is the number of atoms, and $r_{\alpha i}$ and $F_{\alpha i}$ are the i component of the position and force vector of atom α.

We plot the viscosity against the long-time diffusion coefficient in Fig. 3(f), from which we observe that as binding energy increases, viscosity increases in a manner that confirms $D \propto \eta^{-1}$ [dotted line in Fig. 3(f)], consistent with the long-time diffusivity being related to the zero-shear viscosity via the Einstein relation. Theoretically, we can estimate the viscosity due to the relaxation of the stickers via $\eta \propto \tau_m$, where τ_m is the corresponding macroscopic relaxation time given by $\tau_m = r_0^2 D^{-1}$. Then it follows that the viscosity changes with the binding energy as $\eta \propto e^{0.5\varepsilon_b}$, which is also verified by the simulations (Fig. 4).

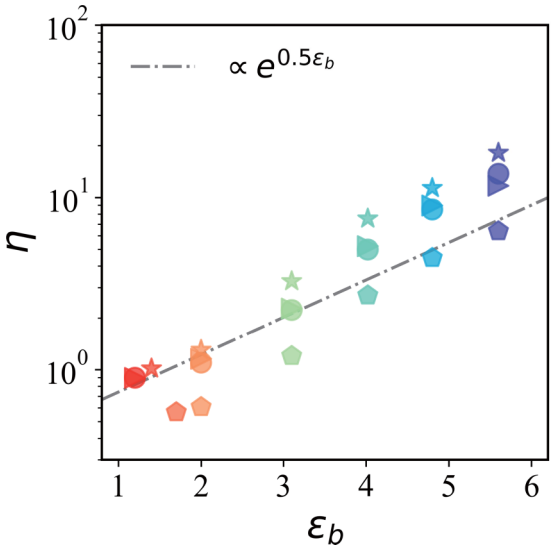

FIG. 4. The zero-shear viscosity increases with the binding energy. Parameters for symbols read as follows: for stars, $m_A = m_B = 6, n = 1.73, \delta = 0$; for triangles, $m_A = 6, m_B = 4, n = 1.73, \delta = 1.4$; for pentagons, $m_A = m_B = 6, n = 1.2, \delta = 0$; and for circles, $m_A = 6, m_B = 4, n = 1.73, \delta = 0$. Colors code for the binding energy.

V. SUMMARY AND DISCUSSION

In this manuscript, we have proposed a way of controlling the dynamics of the liquid condensates in the weak-binding regime. By combining the MD simulations and mean-field theory based on the sticker-spacer model, we reveal that the long-time diffusivity and the macroscopic viscosity of the network liquids correlate with the free sticker fraction, whereby the internal dynamics slows down as the binding strength increases due to the gradual loss of free stickers, i.e., $D \propto W_f \propto e^{-0.5\varepsilon_b}$ and $\eta \propto D^{-1} \propto e^{0.5\varepsilon_b}$. We term the mechanism as the free-sticker-dominated diffusivity. At first glance, the mechanism might seem odd, as it indicates that the macroscopic relaxation time is dictated by the shortest microscopic time τ_0 rather than the longer bond relaxation time τ. In the weak-binding regime, thermodynamic equilibrium is ensured by the fast internal dynamics, thus making the average free sticker fraction relevant to the macroscopic dynamics. In contrast, in the strong-binding regime, breakage of old bonds is correlated to forming of new ones, the diffusivity thus depends strongly on the effective bond lifetime [34], viz., $D \propto \tau^{-1}$.

The difference in the underlying mechanisms between the weak- and strong-binding regime deepens our understanding of the dynamics of the liquid condensates. Our predictions are relevant to condensates with fast internal dynamics. For example, the molecular interactions among intrinsically disordered proteins (IDPs) are transient and dynamic, allowing for rapid exchange of binding partners [42] and thus local thermodynamic equilibrium. In addition, IDPs are typically enriched in charged and polar residues and can form liquid condensates through complex coacervation, wherein the pairwise association condition can be met by controlling the salt concentration [24,42,43]. Weak specific interactions are sufficient to drive LLPS (see Appendix A), whereas strongly associative interactions result in dynamically metastable dimers, oligomers, and microgels [38,44]. In our work, we delineate how the structure and dynamics of the liquid condensates are mediated by the sticker-sticker interactions. Proteins that drive intracellular LLPS encompass both weakly associative low-complexity domains and specific RNA-binding domains [3,24,45], of which the interaction strength is also modified by salt concentration, pH, mutations, and post-translational modifications [11,22,46,47]. Besides, there are interplays between inter- and intramolecular associations controlled by factors like RNA [48] and the high concentrations in the dense phase and the high degree of polymerization might induce entanglements, which lead to slowing independent of bonds (see Appendix B).

Despite that, the binding energy and valence are unknown *a priori*; instead, they can be estimated in the framework of phase separation of associative polymers. The associative interactions mediated by complementary stickers are heterotypic interactions that induce complex coacervation. The concentrations of the coexisting phases are determined by the shape of the multidimentional phase diagram and the total concentrations of the components [14]. Accordingly, one can determine the apparent intersticker binding strength and the effective stoichiometries either theoretically [49] or from simulations [50]. The longtime diffusion coefficient and the zero-shear viscosity of the condensates can be measured via the passive and active microrheology [16].

ACKNOWLEDGMENTS

This work is supported by the National Natural Science Foundation of China under Grants No. 12274212, No. 11974175, and No. 12174184. We are grateful to the High Performance Computing Center (HPCC) of Nanjing University for performing the numerical calculations in this paper on its blade cluster system.

APPENDIX A: LIQUID-LIQUID PHASE SEPARATION DRIVEN BY WEAK SPECIFIC INTERACTIONS

Molecular interactions that drive liquid-liquid phase separation include both specific interactions between complementary stickers and nonspecific interactions between spacers and solvents [24]. In our article, however, we only consider the interactions among stickers that engage in physical crosslinks. Chances are that the phase-separated condensates can result from solely specific interactions. Thus, we perform new MD simulations and use the slab method [44] to determine the concentrations of the coexisting phases.

The equilibrium configuration for $m_{A,B} = 30, \delta = 0, \varepsilon_b = 3.1$ is shown in Fig. 5(a), of which the total concentration of the dense and dilute phase are $n_1 = 0.45, n_2 = 0.17$, respectively, and the relative concentration of the two components in both phases vanishes.

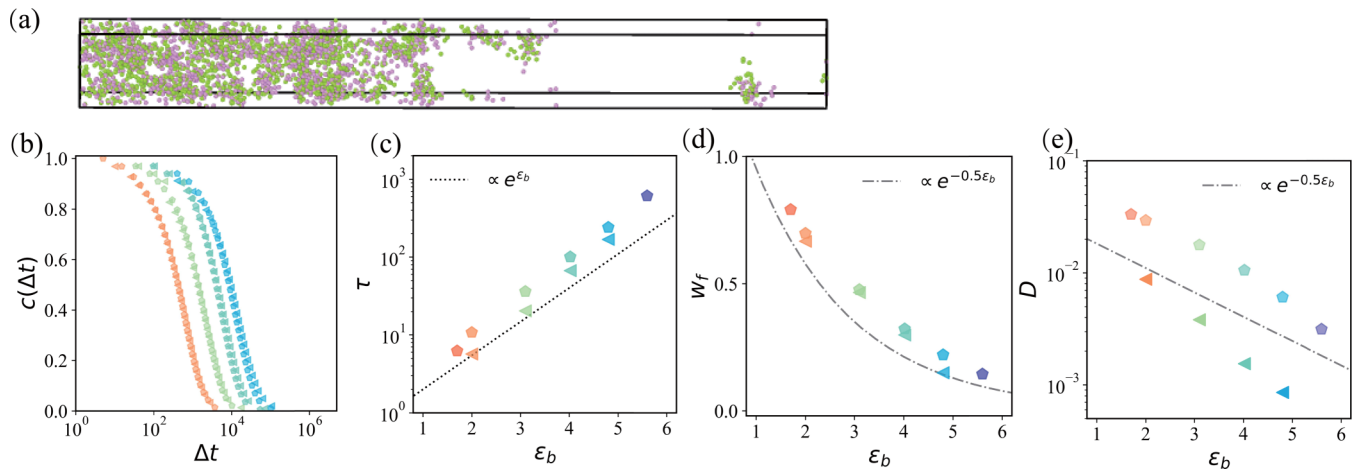

FIG. 5. (a) Snapshot of a simulation with $m_A = m_B = 30$, $\delta = 0$, $\varepsilon_b = 3.1$. (b) Normalized average autocorrelation as a function of lag time. (c) Bond lifetime, (d) free sticker fraction, and (e) the diffusion coefficient as a function of the binding energy. Parameters for (b)–(e): For pentagons, $m_A = m_B = 6$, $n = 1.2$, $\delta = 0$; for left triangles, $m_A = m_B = 30$, $n = 1.2$, $\delta = 0$. Colors code for the binding energy.

APPENDIX B: EFFECTS OF CHAIN LENGTH ON DYNAMICS OF CONDENSATES

We also perform MD simulations at density $n_A = n_B = 0.6$ with $m_A = m_B = 30$ and varying binding energy to study the effects of large chain length on the bulk dynamics. We find that there is no difference in the relaxation of bonds between the systems with small chain length [$m_A = m_B = 6$, pentagons in Fig. 5(b)] and large chain length [left triangles in Fig. 5(b)]. In concordance with that, the bond relaxation time estimated via Eq. (23) is almost the same for both cases [Fig. 5(c)]. Besides, the effect of chain length on the free sticker fraction is negligible [Fig. 5(d)]. However, the average diffusivity of stickers becomes smaller than the free-sticker-dominated diffusivity and deviates from our prediction given by Eq. (17) [indicated by the dash-dotted line in Fig. 5(e)]. Such slowdown in bulk dynamics independent of bonds might correspond to entanglements. On the contrary, the bulk diffusivity confirms the free-sticker-dominated diffusivity if lack thereof [stars and circles in Fig. 3(e)].

[1] S. F. Banani, H. O. Lee, A. A. Hyman, and M. K. Rosen, Biomolecular condensates: Organizers of cellular biochemistry, Nat. Rev. Mol. Cell Biol. **18**, 285 (2017).

[2] C. P. Brangwynne, C. R. Eckmann, D. S. Courson, A. Rybarska, C. Hoege, J. Gharakhani, F. Julicher, and A. A. Hyman, Germline p granules are liquid droplets that localize by controlled dissolution/condensation, Science **324**, 1729 (2009).

[3] M. Feric, N. Vaidya, T. S. Harmon, D. M. Mitrea, L. Zhu, T. M. Richardson, R. W. Kriwacki, R. V. Pappu, and C. P. Brangwynne, Coexisting liquid phases underlie nucleolar subcompartments, Cell **165**, 1686 (2016).

[4] B. A. Gibson, L. K. Doolittle, M. W. G. Schneider, L. E. Jensen, N. Gamarra, L. Henry, D. W. Gerlich, S. Redding, and M. K. Rosen, Organization of chromatin by intrinsic and regulated phase separation, Cell **179**, 470 (2019).

[5] Y. Shin and C. P. Brangwynne, Liquid phase condensation in cell physiology and disease, Science **357**, eaaf4382 (2017).

[6] I. Alshareedah, G. M. Thurston, and P. R. Banerjee, Quantifying viscosity and surface tension of multicomponent protein-nucleic acid condensates, Biophys. J. **120**, 1161 (2021).

[7] S. Boeynaems, A. S. Holehouse, V. Weinhardt, D. Kovacs, J. Van Lindt, C. Larabell, L. Van Den Bosch, R. Das, P. S. Tompa, R. V. Pappu, and A. D. Gitler, Spontaneous driving forces give rise to protein-RNA condensates with coexisting phases and complex material properties, Proc. Natl. Acad. Sci. USA **116**, 7889 (2019).

[8] C. P. Brangwynne, T. J. Mitchison, and A. A. Hyman, Active liquid-like behavior of nucleoli determines their size and shape in xenopus laevis oocytes, Proc. Natl. Acad. Sci. USA **108**, 4334 (2011).

[9] L. B. Case, X. Zhang, J. A. Ditlev, and M. K. Rosen, Stoichiometry controls activity of phase-separated clusters of actin signaling proteins, Science **363**, 1093 (2019).

[10] S. Elbaum-Garfinkle, Y. Kim, K. Szczepaniak, C. C. Chen, C. R. Eckmann, S. Myong, and C. P. Brangwynne, The disordered P granule protein LAF-1 drives phase separation into droplets with tunable viscosity and dynamics, Proc. Natl. Acad. Sci. USA **112**, 7189 (2015).

[11] T. M. Franzmann, M. Jahnel, A. Pozniakovsky, J. Mahamid, A. S. Holehouse, E. Nuske, D. Richter, W. Baumeister, S. W. Grill, R. V. Pappu, A. A. Hyman, and S. Alberti, Phase separation of a yeast prion protein promotes cellular fitness, Science **359**, eaao5654 (2018).

[12] L. M. Jawerth, M. Ijavi, M. Ruer, S. Saha, M. Jahnel, A. A. Hyman, F. Julicher, and E. Fischer-Friedrich, Salt-Dependent Rheology and Surface Tension of Protein Condensates using Optical Traps, Phys. Rev. Lett. **121**, 258101 (2018).

[13] M. C. Munder, D. Midtvedt, T. Franzmann, E. Nuske, O. Otto, M. Herbig, E. Ulbricht, P. Muller, A. Taubenberger, S. Maharana, L. Malinovska, D. Richter, J. Guck, V. Zaburdaev, and S. Alberti, A pH-driven transition of the cytoplasm from a

fluid- to a solid-like state promotes entry into dormancy, eLife **5**, e09347 (2016).

[14] S. Saha, C. A. Weber, M. Nousch, O. Adame-Arana, C. Hoege, M. Y. Hein, E. Osborne-Nishimura, J. Mahamid, M. Jahnel, L. Jawerth, A. Pozniakovski, C. R. Eckmann, F. Julicher, and A. A. Hyman, Polar positioning of phase-separated liquid compartments in cells regulated by an mRNA competition mechanism, Cell **166**, 1572 (2016).

[15] H. Zhang, S. Elbaum-Garfinkle, E. M. Langdon, N. Taylor, P. Occhipinti, A. A. Bridges, C. P. Brangwynne, and A. S. Gladfelter, RNA controls polyQ protein phase transitions, Mol. Cell **60**, 220 (2015).

[16] L. Jawerth, E. Fischer-Friedrich, S. Saha, J. Wang, T. Franzmann, X. Zhang, J. Sachweh, M. Ruer, M. Ijavi, S. Saha, J. Mahamid, A. A. Hyman, and F. Julicher, Protein condensates as aging Maxwell fluids, Science **370**, 1317 (2020).

[17] M. Kato, T. W. Han, S. Xie, K. Shi, X. Du, L. C. Wu, H. Mirzaei, E. J. Goldsmith, J. Longgood, J. Pei, N. V. Grishin, D. E. Frantz, J. W. Schneider, S. Chen, L. Li, M. R. Sawaya, D. Eisenberg, R. Tycko, and S. L. McKnight, Cell-free formation of RNA granules: Low complexity sequence domains form dynamic fibers within hydrogels, Cell **149**, 753 (2012).

[18] S. Maharana, J. Wang, D. K. Papadopoulos, D. Richter, A. Pozniakovsky, I. Poser, M. Bickle, S. Rizk, J. Guillen-Boixet, T. M. Franzmann, M. Jahnel, L. Marrone, Y. T. Chang, J. Sterneckert, P. Tomancak, A. A. Hyman, and S. Alberti, RNA buffers the phase separation behavior of prion-like RNA binding proteins, Science **360**, 918 (2018).

[19] Y. Shin, J. Berry, N. Pannucci, M. P. Haataja, J. E. Toettcher, and C. P. Brangwynne, Spatiotemporal control of intracellular phase transitions using light-activated optodroplets, Cell **168**, 159 (2017).

[20] S. Alberti and D. Dormann, Liquid-liquid phase separation in disease, Annu. Rev. Genet. **53**, 171 (2019).

[21] S. Alberti and A. A. Hyman, Biomolecular condensates at the nexus of cellular stress, protein aggregation disease and ageing, Nat. Rev. Mol. Cell Biol. **22**, 196 (2021).

[22] A. Patel, H. O. Lee, L. Jawerth, S. Maharana, M. Jahnel, M. Y. Hein, S. Stoynov, J. Mahamid, S. Saha, T. M. Franzmann, A. Pozniakovski, I. Poser, N. Maghelli, L. A. Royer, M. Weigert, E. W. Myers, S. Grill, D. Drechsel, A. A. Hyman, and S. Alberti, A liquid-to-solid phase transition of the als protein fus accelerated by disease mutation, Cell **162**, 1066 (2015).

[23] A. Yamasaki, J. M. Alam, D. Noshiro, E. Hirata, Y. Fujioka, K. Suzuki, Y. Ohsumi, and N. N. Noda, Liquidity is a critical determinant for selective autophagy of protein condensates, Mol. Cell **77**, 1163 (2020).

[24] C. P. Brangwynne, P. Tompa, and R. V. Pappu, Polymer physics of intracellular phase transitions, Nat. Phys. **11**, 899 (2015).

[25] J. Nikolic, R. Le Bars, Z. Lama, N. Scrima, C. Lagaudriere-Gesbert, Y. Gaudin, and D. Blondel, Negri bodies are viral factories with properties of liquid organelles, Nat. Commun. **8**, 58 (2017).

[26] J. Wang, J. M. Choi, A. S. Holehouse, H. O. Lee, X. Zhang, M. Jahnel, S. Maharana, R. Lemaitre, A. Pozniakovsky, D. Drechsel, I. Poser, R. V. Pappu, S. Alberti, and A. A. Hyman, A molecular grammar governing the driving forces for phase separation of prion-like RNA binding proteins, Cell **174**, 688 (2018).

[27] A. Bremer, M. Farag, W. M. Borcherds, I. Peran, E. W. Martin, R. V. Pappu, and T. Mittag, Deciphering how naturally occurring sequence features impact the phase behaviours of disordered prion-like domains, Nat. Chem. **14**, 196 (2022).

[28] J. M. Choi, A. S. Holehouse, and R. V. Pappu, Physical principles underlying the complex biology of intracellular phase transitions, Annu. Rev. Biophys. **49**, 107 (2020).

[29] T. S. Harmon, A. S. Holehouse, M. K. Rosen, and R. V. Pappu, Intrinsically disordered linkers determine the interplay between phase separation and gelation in multivalent proteins, eLife **6**, e30294 (2017).

[30] P. Li, S. Banjade, H. C. Cheng, S. Kim, B. Chen, L. Guo, M. Llaguno, J. V. Hollingsworth, D. S. King, S. F. Banani, P. S. Russo, Q. X. Jiang, B. T. Nixon, and M. K. Rosen, Phase transitions in the assembly of multivalent signalling proteins, Nature (London) **483**, 336 (2012).

[31] E. W. Martin, A. S. Holehouse, I. Peran, M. Farag, J. J. Incicco, A. Bremer, C. R. Grace, A. Soranno, R. V. Pappu, and T. Mittag, Valence and patterning of aromatic residues determine the phase behavior of prion-like domains, Science **367**, 694 (2020).

[32] A. N. Semenov and M. Rubinstein, Thermoreversible gelation in solutions of associative polymers. 1. statics, Macromolecules **31**, 1373 (1998).

[33] M. T. Wei, S. Elbaum-Garfinkle, A. S. Holehouse, C. C. Chen, M. Feric, C. B. Arnold, R. D. Priestley, R. V. Pappu, and C. P. Brangwynne, Phase behaviour of disordered proteins underlying low density and high permeability of liquid organelles, Nat. Chem. **9**, 1118 (2017).

[34] P. Ronceray, Y. Zhang, X. Liu, and N. S. Wingreen, Stoichiometry Controls the Dynamics of Liquid Condensates of Associative Proteins, Phys. Rev. Lett. **128**, 038102 (2022).

[35] S. Plimpton, Fast parallel algorithms for short-range molecular-dynamics, J. Comput. Phys. **117**, 1 (1995).

[36] P. J. Flory, Molecular size distribution in three dimensional polymers. I. Gelation, J. Am. Chem. Soc. **63**, 3083 (1941).

[37] W. H. Stockmayer, Theory of molecular size distribution and gel formation in branched-chain polymers, J. Chem. Phys. **11**, 45 (1943).

[38] S. Ranganathanand E. I. Shakhnovich, Dynamic metastable long-living droplets formed by sticker-spacer proteins, eLife **9**, e56159 (2020).

[39] K. Sozanski, A. Wisniewska, T. Kalwarczyk, and R. Holyst, Activation Energy for Mobility of Dyes and Proteins in Polymer Solutions: From Diffusion of Single Particles to Macroscale Flow, Phys. Rev. Lett. **111**, 228301 (2013).

[40] K. Makuch, R. Holyst, T. Kalwarczyk, P. Garstecki, and J. F. Brady, Diffusion and flow in complex liquids, Soft Matter **16**, 114 (2020).

[41] B. D. Todd and P. J. Daivis, *Nonequilibrium Molecular Dynamics: Theory, Algorithms and Applications* (Cambridge University Press, 2017).

[42] P. E. Wright and H. J. Dyson, Intrinsically disordered proteins in cellular signalling and regulation, Nat. Rev. Mol. Cell Biol. **16**, 18 (2015).

[43] V. N. Uversky, I. M. Kuznetsova, K. K. Turoverov, and B. Zaslavsky, Intrinsically disordered proteins as crucial constituents of cellular aqueous two phase systems and coacervates, FEBS Lett. **589**, 15 (2015).

[44] Y. Zhang, B. Xu, B. G. Weiner, Y. Meir, and N. S. Wingreen, Decoding the physical principles of two-component biomolecular phase separation, eLife **10**, e62403 (2021).

[45] H. B. Schmidt and D. Gorlich, Nup98 FG domains from diverse species spontaneously phase-separate into particles with nuclear pore-like permselectivity, eLife **4**, e04251 (2015).

[46] A. Agarwal, S. K. Rai, A. Avni, and S. Mukhopadhyay, An intrinsically disordered pathological prion variant Y145stop converts into self-seeding amyloids via liquid-liquid phase separation, Proc. Natl. Acad. Sci. USA **118**, e2100968118 (2021).

[47] Z. T. Monahan, V. H. Ryan, A. M. Janke, K. A. Burke, S. N. Rhoads, G. H. Zerze, R. N. o Meally, G. L. Dignon, A. E. Conicella, W.-w. Zheng, R. B. Best, R. N. Cole, J. Mittal, F. Shewmaker, and N. L. Fawzi, Phosphorylation of the fus low-complexity domain disrupts phase separation, aggregation, and toxicity, EMBO J. **36**, 2951 (2017).

[48] J. Guillén-Boixet, A. Kopach, A. S. Holehouse, S. Wittmann, M. Jahnel, R. Schlüßler, K. Kim, I. R. Trussina, J. Wang, D. Mateju *et al.*, RNA-induced conformational switching and clustering of G3BP drive stress granule assembly by condensation, Cell **181**, 346 (2020).

[49] D. Prusty, V. Pryamitsyn, and M. Olvera de la Cruz, Thermodynamics of associative polymer blends, Macromolecules **51**, 5918 (2018).

[50] J.-M. Choi, F. Dar, and R. V. Pappu, Lassi: A lattice model for simulating phase transitions of multivalent proteins, PLoS Comput. Biol. **15**, e1007028 (2019).